

Spatiotemporal Synchronization of Drift Waves in a Magnetron Sputtering Plasma

E. Martines¹, M. Zuin¹, R. Cavazzana¹, J. Adámek², V. Antoni¹, G. Serianni¹, M. Spolaore¹, N. Vianello¹

¹*Consorzio RFX, Associazione EURATOM-ENEA sulla Fusione, Padova, Italy*

²*Institute of Plasma Physics AS CR, Prague, Czech Republic*

(Dated: June 17, 2021)

A feedforward scheme is applied for drift waves control in a magnetized magnetron sputtering plasma. A system of driven electrodes collecting electron current in a limited region of the explored plasma is used to interact with unstable drift waves. Drift waves actually appear as electrostatic modes characterized by discrete wavelengths of the order of few centimeters and frequencies of about 100 kHz. The effect of external quasi-periodic, both in time and space, travelling perturbations is studied. Particular emphasis is given to the role played by the phase relation between the natural and the imposed fluctuations. It is observed that it is possible by means of localized electrodes, collecting currents which are negligible with respect to those flowing in the plasma, to transfer energy to one single mode and to reduce that associated to the others. Due to the weakness of the external action, only partial control has been achieved.

I. INTRODUCTION

Active control of plasma fluctuations is a line of research which has potentially important implications for controlled thermonuclear fusion activities. Active magnetic coils have been, indeed, widely and successfully used in fusion devices for MHD control, and an electrostatic approach has been recently proposed with the aim of inducing given harmonics on the global equilibrium by means of distributed electrodes at the edge plasma [1]. Moreover, at the plasma edge, electrostatic fluctuations of various nature are believed to be responsible for cross-field energy and particle transport processes in fusion devices. For example, it has been shown in a linear machine that by driving one of the drift wave modes present in the plasma the background turbulence level can be reduced [2]. More recently, also the nonlinear interaction of drift waves with externally driven currents has been investigated [3]. The synchronization of dust acoustic waves in a dusty plasma has been also successfully achieved using a negatively biased driving electrode [4]. In the Large Plasma Device (LAPD) the gradient-driven instability has been suppressed by the beating of two independent externally driven shear-Alfvén waves [5].

In this paper the first attempt of synchronizing naturally occurring electrostatic fluctuations to an externally applied resonant pattern in a low temperature magnetron plasma is described. Magnetrons are plasma sputtering devices widely used for thin film deposition applications. They can be broadly divided into two categories, cylindrical and planar magnetrons. In both types, a glow discharge is established between a cathode and an anode in the presence of a magnetic field confining the electrons in a plasma region with a relatively high density and ionization rate. A high flux of ions is thus created by ionization of the working gas and accelerated towards the cathode to induce the sputtering of a target placed over it.

A range of electrostatic fluctuations has been observed in cylindrical and planar magnetron plasmas, powered in DC [6–8], in a pulsed way [9] and at radiofrequency [10]. The main aim of studying fluctuation phenomena in such

plasmas is to explain the cross-field transport rate and its role in the efficiency of the plasma processes involved. As said above, this would have an interest not only for the applicative perspective of improving the deposition rate, but also for plasma physics in general. In fusion plasmas, for example, fluctuations driven by a wide kind of unstable modes are believed to be at the origin of confinement degradation [11].

This paper is devoted to the description of the results of an experimental activity aimed at synchronizing spontaneous electrostatic instabilities by means of localized electrodes immersed in a magnetron plasma. The paper is organized as follows. Section II is devoted to the description of the experimental setup, section III to the description and the discussion of the experimental results. Conclusion are then presented. In the Appendix the deduction of the linear dispersion relation for the instability under investigation is given.

II. EXPERIMENTAL SETUP

The experimental activity here described has been performed on a planar magnetron sputtering device, whose layout is shown in Fig. 1, constituted by a stainless steel vacuum chamber (500 mm height and 400 mm diameter) and by a sputtering source (the cathode), 10 cm diameter, placed at the bottom of the vacuum chamber itself; z is the vertical source axis, with its origin on the target upper surface and directed upward, and r the radial coordinate. The device has been operated with a DC power supply and Argon as filling gas. The magnetic field above the source is provided by 24 pairs of permanent magnets circularly equally spaced at about 50 mm from the axis, plus a further pair placed in the center. Lateral magnets have a magnetic polarization opposite to that of the central pair. In Fig. 1 a detail of the location of the magnets and of the magnetic field map above the magnetron source is also shown. The magnets are placed under the target in a water cooled copper bulk, and an iron plate is placed under them.

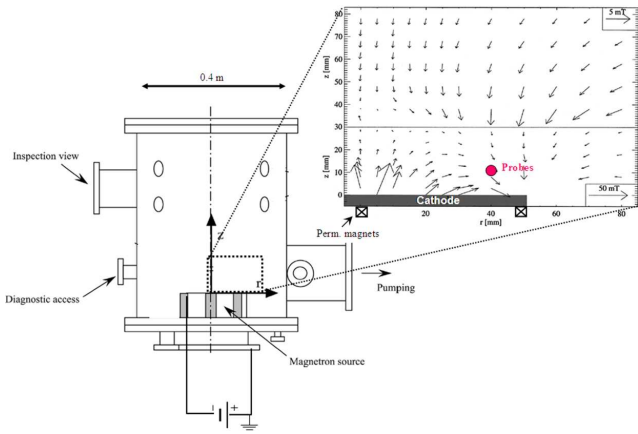


FIG. 1: Scheme of the magnetron sputtering device, with a detail of the plasma region under investigation showing the map of the magnetic field lines and the location of the probes.

In order to investigate the spatial and temporal plasma fluctuation dynamics a diagnostic tool had been developed, as described in Ref. [13]. This diagnostic system consists of 16 equally spaced Langmuir probes forming a circular array with a radius of 40 mm. Each probe electrode is a stainless steel cylinder, 1.5 mm in radius and 1 mm long, connected to a stainless steel wire with 0.8 mm diameter, for a total collecting area of about 16 mm². The wire is housed in a quartz tube, having inner and outer radii of 1 mm and 3 mm and a length of 120 mm. The probes are kept in place by means of an aluminum disc, which acts as supporting structure. As shown in Fig. 2, the system was placed coaxially with the cylindrical vacuum chamber, with the probes located on a plane parallel to the cathode surface at $z = 13$ mm, such position being indicated also in Fig. 1. The position was chosen consistently with the diagnostics described in Refs. [12, 13].

The active control system consists of 8 electrodes placed at the same z and radial position of the probes. The electrodes are U -shaped stainless steel cylinders (see Fig. 2), 1 mm diameter, 35 mm long, for a total collecting area of 110 mm², which is almost one order of magnitude larger than the probe area. As shown in Fig. 3, the 8 electrodes used as drivers are azimuthally displaced so that each electrode lays between two adjacent probes.

It is important to note that this layout has been chosen to obtain a drive system which is local, affecting only half of the domain. This is an important condition, which differentiates our control experiments from previous ones, where almost the whole plasma volume was affected by equally distributed active electrodes [2, 3].

The fluctuation measurements are collected by connecting the probes to ground through a resistance chosen to be 1 k Ω , and measuring the potential fall δV on the resistance itself. Such configuration, which puts our measurement in between the real floating potential value

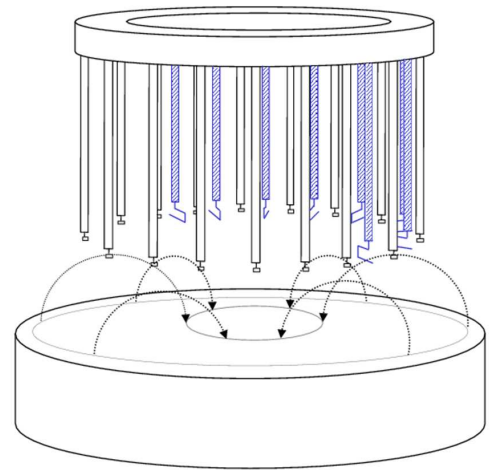


FIG. 2: Scheme of the diagnostic and of the active control electrodes apparatus disposed above the cathode surface at $z = 13$ mm. The electrodes can be recognized for their U-shape. Dashed curves represent the magnetic field lines intersecting the plasma region under investigation.

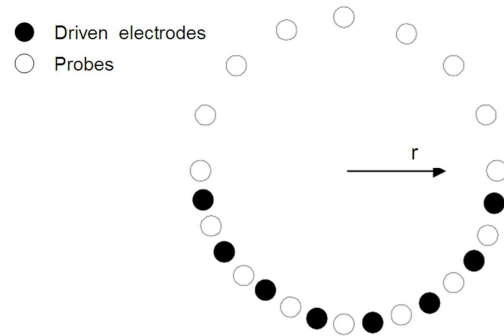


FIG. 3: Probes and driven electrodes distribution, as seen from above.

and the negative potential for the ion saturation current on the Langmuir characteristics, must be considered as a compromise to obtain a larger frequency bandwidth (usually attainable by measuring the ion saturation current fluctuations) without the use of high voltage power supplies for such a large number of probes. Due to the closeness of such measurement to the floating potential value, we will hereafter name it V_f . The data were collected by means of a digital oscilloscope with isolated inputs, sampled at 2 MHz with 12-bit resolution using the oscilloscope itself. Records of 200 ksamples were captured. The chosen values for the two main control parameters, namely the discharge current and the neutral gas pressure are $I = 0.6$ A and $P = 1$ Pa, respectively, corresponding to a discharge power of 260 W.

Regarding the control system, the scheme adopted in these experiments allows to create in the 8 drivers a travelling pattern with a defined azimuthal periodicity at a

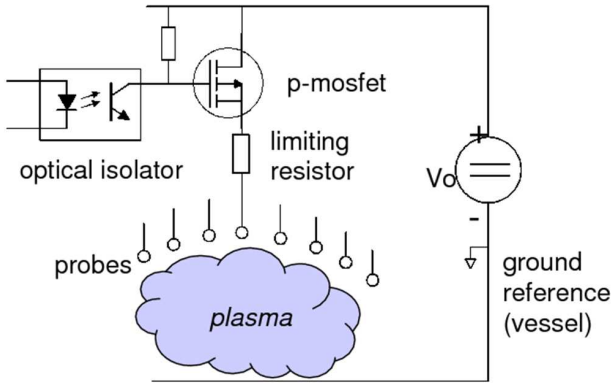


FIG. 4: Scheme of principle of the electrodes driving system.

chosen frequency. This is performed, in practice, by connecting in sequence each electrode to a power supply delivering a constant voltage V_d larger than the floating potential using a Mosfet. The Mosfets are controlled by a programmable function generator, so as to create the correct spatiotemporal pattern. In this way, a train of positive (i.e. from the probe to the plasma) current peaks is created, forming a perturbation with the appropriate wavenumber and frequency. The wave is clearly non-sinusoidal, and indeed this approach was chosen having recognized that only driving the probe to voltages higher than the floating potential, towards the electron part of the $I - V$ characteristic, yields a substantial current. A scheme of principle of the driving system is reported in Fig. 4.

It is important to observe here that, due to the rather small collecting surfaces of the probes, only small currents (of the order of few mA) can be drawn, so that the applied perturbation is weak ($\leq 1\%$) when compared to the global discharge properties.

III. EXPERIMENTAL RESULTS

In Fig. 5 the horizontal profiles of the time averaged plasma parameters at $z = 13$ mm, i.e. in the position of the probes and the driven electrodes, namely plasma potential V_p , electron density n_e and temperature T_e , as measured and described in [13], are shown. These data are given for completeness. Indeed, they are a key ingredient in the theoretical interpretation of the fluctuation phenomena we are here trying to control in terms of drift waves [12, 13].

The density radial profile is found to be peaked at $r \sim 30$ mm, inside the magnetic trap, where the plasma potential has a minimum, which is different from what obtained in other magnetron devices [15]. The electron temperature inside the trap is in the range 1.4 - 2 eV, without any clear dependence on the radial coordinate (ions are at room temperature). It is worth to note that,

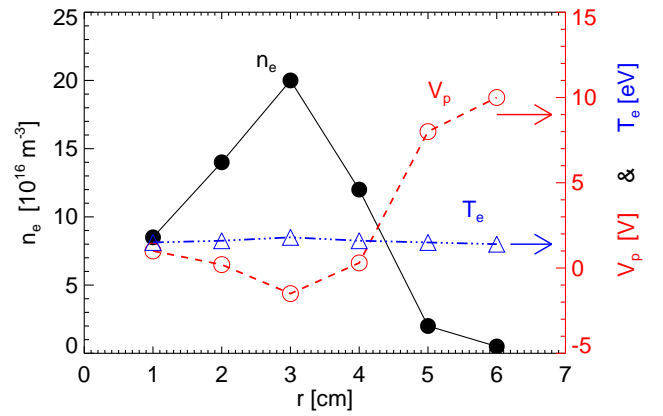


FIG. 5: Radial profiles of electron density n_e (full dots), temperature T_e (circles) and plasma potential V_p (triangles) measured at $z = 13$ mm from the cathode surface. The two latter quantities refer to the righthand side y-axis.

as typical of this kind of plasmas, the electrons have been observed to be characterized not by a simple Maxwellian distribution, but by the superposition of two main populations at different energies. The colder component, the one we are referring to in this paper, is the dominant one in terms of particle number. The hotter component of the electron distribution has an electron temperature of about 15 eV at a density that is about three orders of magnitude lower than the colder one [14].

Turning now to the fluctuation measurements, we report here (see Fig. 6) an example of the spectra obtained from one of the 16 probes composing the azimuthal array. The spectrum is found to be characterized by the presence of few coherent peaks in the frequency range between 10 and 200 kHz, more pronounced above 80 kHz. The higher frequency part of the spectrum exhibits a power law decay, $f^{-\alpha}$, with the spectral index $\alpha \simeq 3.6$.

By means of the full array of 16 probes the dispersion relation (i.e. the relation between the frequency peaks and the corresponding wave numbers) along the azimuthal direction can be deduced. In Fig. 7 the $S(k, f)$ spectrum is shown in a color-coded contour, the color being associated (in a.u.) to the spectral density. The azimuthal component of the wavevector k_y is actually expressed in terms of the mode number $m = k_y r$, being r the radius at which the measurements are taken. It is evident that the three dominant frequency peaks, at $f > 60$ kHz, correspond to different azimuthal Fourier modes, with $m = 3, 4, 5$ ($m = 6$ and $m = 7$ are also slightly visible). Along with the part of spectrum propagating in the electron diamagnetic direction an important $m = 0$ component is present, exhibiting a broadband activity superposed to a peak located at around 20 kHz and to its higher harmonics.

The overplotted curve is the theoretical linear disper-

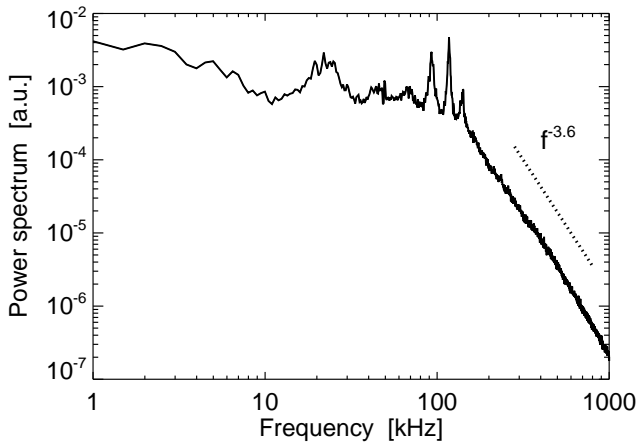


FIG. 6: Power spectrum deduced from a single V_f probe signal. A power law interpolation ($f^{-\alpha}$, with $\alpha \simeq 3.6$) of the high frequency part of the spectrum is proposed as a dashed line.

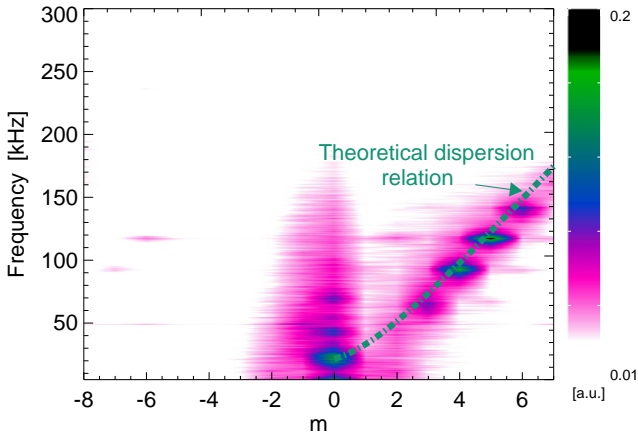


FIG. 7: Contour plot of the frequency and wavenumber resolved spectrum $S(m, f)$ of the fluctuation. The superimposed dashed curve represents the dispersion relation given by eq. 1.

sion relation:

$$\omega^2 + \omega \left[\frac{\Omega_i}{\nu_i} (k_x - \frac{\Omega_i}{\nu_i} k_y) v_E + i(\nu_i - Z) \right] - k^2 C_s^2 + Z \nu_i - i \Omega_i \left[\left(\frac{\Omega_i}{\nu_i} k_y - k_x \right) v_E + k_x v_{de} \right] = 0 \quad (1)$$

whose deduction, exposed in refs. [12, 13], is briefly resumed in the Appendix. Here C_s is the ion sound velocity, $C_s \simeq (T_e/m)^{1/2}$, v_E is the $\mathbf{E} \times \mathbf{B}$ velocity, ν_i is the collision frequency of ions with neutrals, Ω_i is the ion cyclotron frequency multiplied by 2π , \mathbf{k} is the wavevector and v_{de} is the electron diamagnetic drift velocity $v_{de} = -T_e/(enB)(dn/dx)$.

The real part of the root of the theoretical dispersion relation, i.e the solution $f = f(k_y)$, being $f = \omega/2\pi$, of this equation is found to be in good agreement with the

experimental peaks for the case considered. Note that the k_x and k_z values are taken as free parameters in a non-linear fit procedure, and that the resulting wavelengths are compatible with the geometry of the chamber and of the magnetic field lines ($\lambda_x \approx 4$ cm and $\lambda_z \approx 20$ cm). A detailed characterization of the properties of the fluctuations in a wide range of neutral gas pressure has been performed and described in Ref. [13], along with a comparison between the linear theoretical growth rate and the observed mode amplitude. The agreement between the theoretical and the experimental dispersion relation allows to interpret the fluctuations under study in terms of a $\mathbf{E} \times \mathbf{B}$ /density gradient instability, also known as *neutral drag* instability.

It must be said that peaks at frequencies of the order of few kHz in the fluctuation power spectrum have been already observed in a DC cylindrical magnetron discharge by Kudrna et al. [8], and at the ion cyclotron frequency by Sheridan and Goree in a planar magnetron system [7]. It is worth to add that the observed instabilities exhibit almost the same properties of those characterizing the plasma of a high power impulse magnetron sputtering, as recently reported [9].

A deeper analysis of the time behavior of the fluctuations reveals that the dynamics of the propagating waves is rather complex, as can be seen in Fig. 8 where the spectrogram of a single probe signal, i.e. the frequency power spectrum resolved in time, shows that the energy related the various peaks is not constant. In particular, the energy of the fluctuation is found to jump over the various mode numbers, whose time resolved amplitude is shown in the bottom panel of Fig. 8.

No regularity can be observed in this process, which suggests that some form of chaotic behavior might be present, as it happens in the case of coupled oscillators. Indeed, chaos induced by electrostatic waves in plasmas has been studied in the recent past [17], and chaos control techniques were proposed and successfully tested in travelling tubes, by building barriers in phase space with small perturbations [16]. A similar situation is also observed in a study of the transition from stability to drift wave turbulence in a magnetized, low temperature, cylindrical plasma, where a state with two broad peaks in the Fourier space is characterized by a spatiotemporal pattern exhibiting temporally localized defects [18].

As said above, the scheme attempted in these experiments is to obtain an active control of the plasma fluctuations in order to induce a more regular fluctuation wavefront by creating in the 8 drivers a travelling pattern with a defined azimuthal periodicity at a chosen frequency. In principle, by this approach, a spatio-temporal voltage pattern which is resonant with the natural propagating modes, can be applied. In particular, the adopted strategy is to drive one single mode with a local electrode system (in contrast with the generally used global systems [18]) to control the whole plasma behavior.

In particular, we decided to operate on the $m = 4$ and $m = 5$ modes at different frequencies. An example of

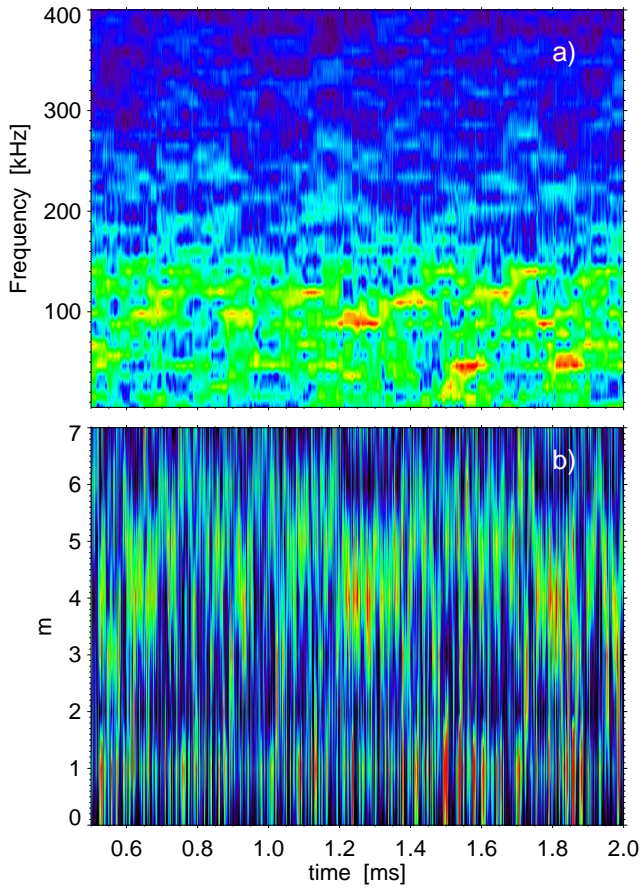


FIG. 8: Color-coded contours of a) spectrogram of a single probe fluctuation and b) time behavior of the modes amplitude.

the pattern of pulses applied to the drivers can be seen in Fig. 9 overplotted (in false units) on the color-coded contour of the probe signals.

An example of what happens to the spectrum when a resonant travelling $m = 4$ mode is applied is shown in Fig. 10. The signal is chosen to be on the opposite half side of the probe array with respect to the half array where also the electrodes lay (see Fig. 3). The spectrum exhibits a sharp peak at the applied frequency and at its higher harmonics, along with a significant reduction of the power associated to the other modes, in particular to that of $m = 0$ mode at around 20 kHz, which appears almost fully depressed. Negligible effect on the high frequency broadband part of the spectrum is observed, differently from what was found in Ref. [2] where a preselected mode was enhanced to the expense of broadband low-frequency spectral components. It is important to say that these results are obtained only with the application of a perturbation which is co-rotating with the natural fluctuations, while a counter-rotating perturbation gives almost no effect. This is shown in Fig. 11, where the spectrogram of the V_f fluctuation is presented for the cases with no external and with a co-rotating and

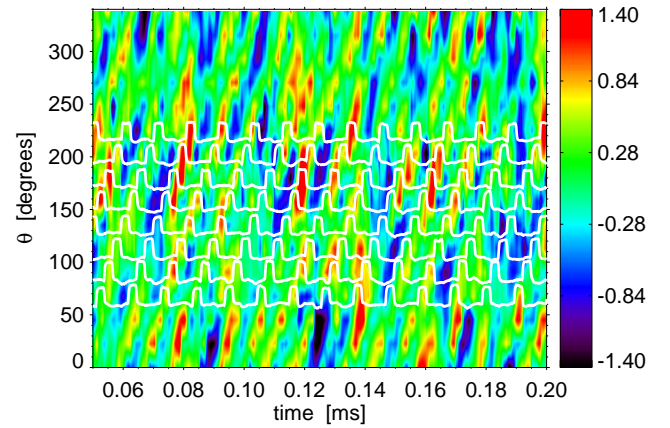


FIG. 9: Contour plot of the time trace of the 16 signals (color scale is in Volts). The overplotted white curves are the voltage signals of the 8 electrodes. A propagating pattern with $m = 4$ periodicity can be observed both on the probes and the electrodes.

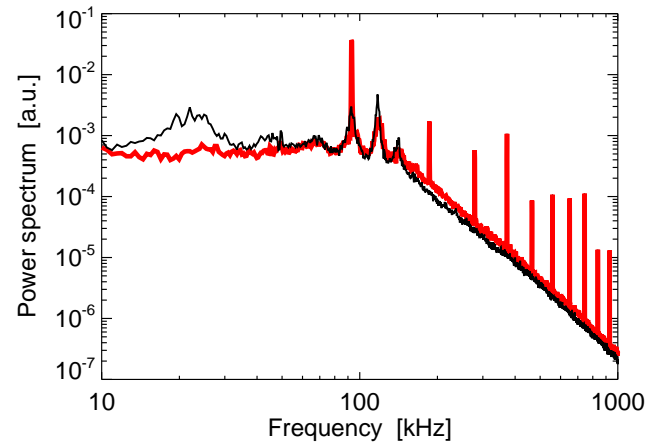


FIG. 10: Power spectrum of a single probe signal for a reference experimental condition (black), i.e. with no current driven on the electrodes, and with an applied $m = 4$ mode at 93 kHz (red). and

a counter-rotating $m = 4$ mode at 95 kHz. Only in Fig. 11(c) (i.e., in the co-rotating case) the induced peak is found to largely affect the full fluctuation spectrum.

Actually the behavior of the peak associated to the induced perturbation is a function of the applied frequency itself and of the corresponding wavelength of the rotating pattern on the drivers. In Fig. 12 the power spectrum of the single floating probe signal is plotted in a color coded contour as a function of the driving frequency, relative to the natural one for the considered mode. It can be observed that the height of the additional sharp peak is a function of the driving frequency; the peak has, indeed, a maximum when the driving frequency equals that of the naturally occurring $m = 4, 5$ mode, i.e. when the perturbation is resonant with the plasma.

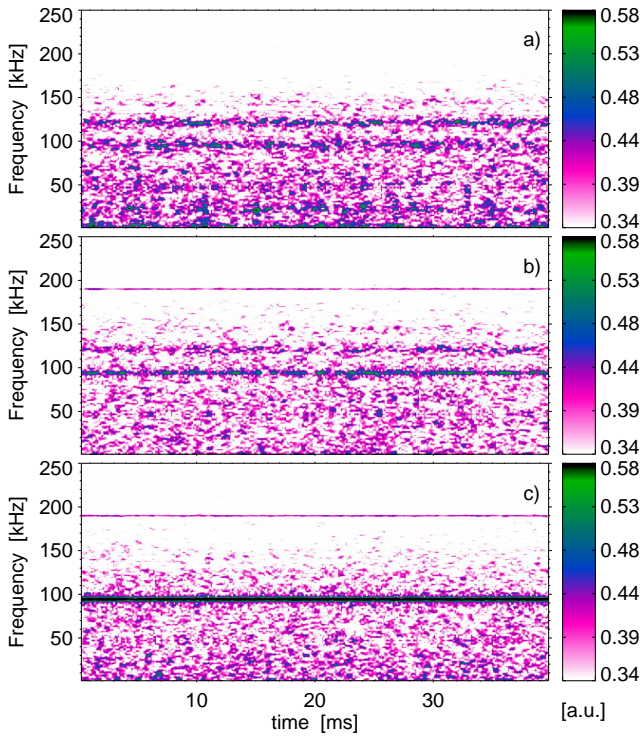


FIG. 11: Color-coded contours of the spectrogram (i.e. power spectrum *vs* time) of a single V_f signal with: a) no external perturbation, b) with a counter rotating $m = 4$ mode and c) with a co-rotating $m = 4$ mode. and

If the height of the additional peak is plotted as a function of the driving frequency, as is shown in Fig. 13, a bell-shaped curve is indeed obtained, which is reminiscent of the response of a resonator. The ratio of the curve width to the peak frequency yields a quality factor $Q = \omega_0/\Delta\omega \approx 10$, depending on the mode number considered.

Turning to the peak in the spectrum associated to the drift-wave mode, it is found that also its energy is strongly dependent on the driven frequency. This is shown in Fig. 14, where the amplitude of the main $m = 0, 3, 4, 5, 6$ modes is shown for various applied frequencies to the driven electrodes (what is actually used is the difference with respect to the natural one), and with a $m = 4$ and a $m = 5$ applied pattern. For both cases, when the natural frequency is matched, i.e. when a resonant condition is achieved, a large enhancement of the mode is found, with part of the energy being taken from the other ones. The system thus seems to be pushed towards a more regular state. As previously deduced from the analysis of the simple $S(f)$ spectrum, a strong effect is confirmed to be found on the $m = 0$ mode, whose amplitude is reduced by a factor two, but also the others not-driven modes exhibit a sensible reduction.

The effect of the perturbation on the plasma, in the resonant condition is displayed in Fig. 15, which shows the phase $\alpha_{drive}(t)$ of the $m = 4$ mode applied to the

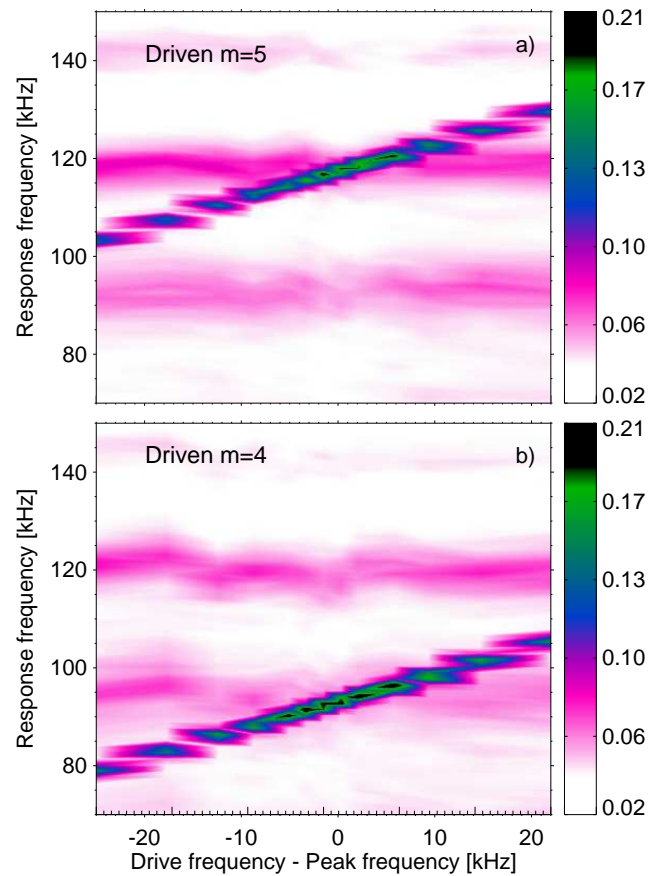


FIG. 12: Power spectra of a single floating potential probe as a function of the driving frequency for an applied $m = 4$ (a) and $m = 5$ (b) mode.

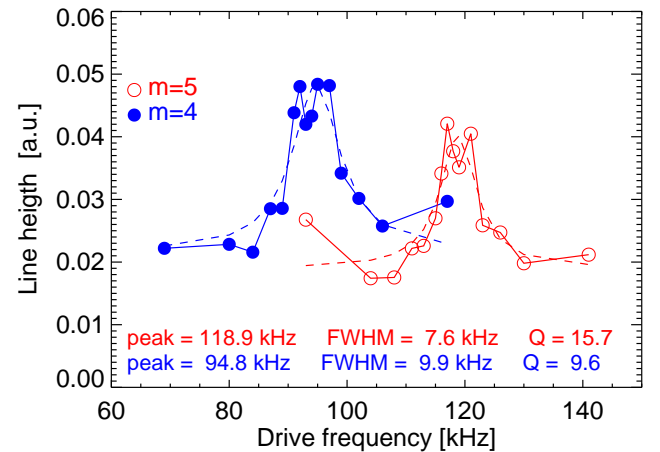


FIG. 13: The eight of the additional peak plotted as a function of the driving frequency for the $m = 4$ (full dots) and $m = 5$ (open circles) mode. Dashed lines represent the Lorentzian interpolation, whose properties (Q factor, FWHM and peak frequency) are also indicated.

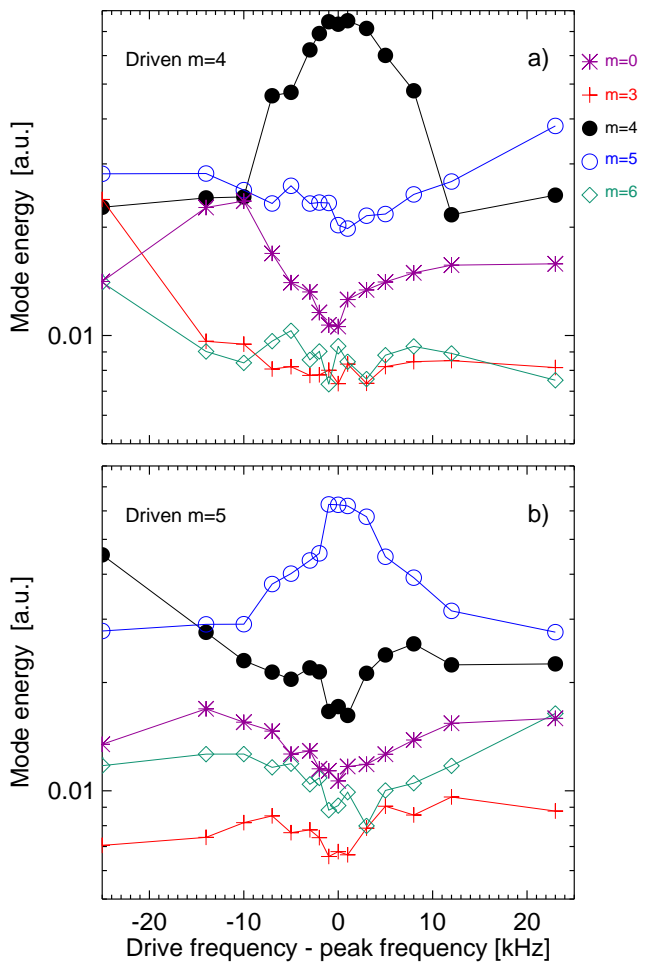


FIG. 14: Energy of the $m = 0, 3, 4, 5, 6$ modes plotted as a function of the frequency difference between drive and spontaneous fluctuation: a) and b) refer to cases with a driven $m = 4$ and $m = 5$ mode, respectively.

drivers (in black) and the phase of the $\alpha_m(t)$ of the $m = 4$ mode as measured by the sensors. It is possible to see, qualitatively, that the drive and the response are synchronized only for a fraction of the time.

This is more clearly seen in Fig. 16, where the phase of the response is plotted versus the phase of the drive for the whole time record. The black vertical stripes are due to the fact that the drive phase does not vary linearly, since the drive is not sinusoidal. Apart from this effect, it is also possible to see a diagonal darker band, which shows that there exists a preferred phase relationship between drive and response. Such relationship however occurs only intermittently, so that some points are present also in other regions of the plot. Indeed, the occurrence of the phase synchronization, as defined by the presence of a preferred value of the drive-response phase difference, is found to depend on the drive frequency. Indeed, the phase difference distribution is more peaked when the drive frequency matches that of the naturally occurring

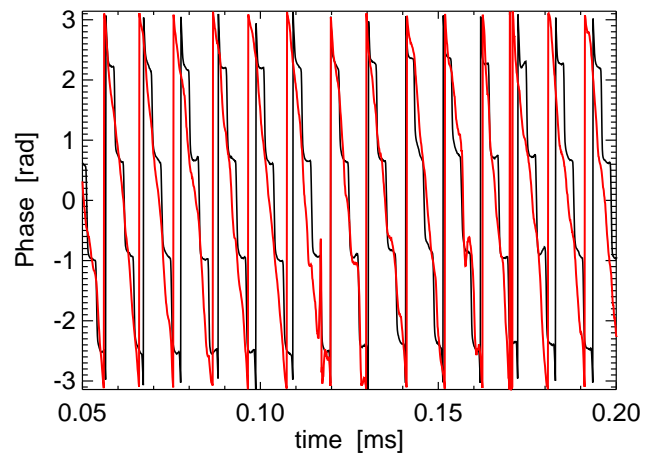


FIG. 15: Time evolution of the phase of the $m = 4$ drive (black) and $m = 4$ response (red) in resonant condition.

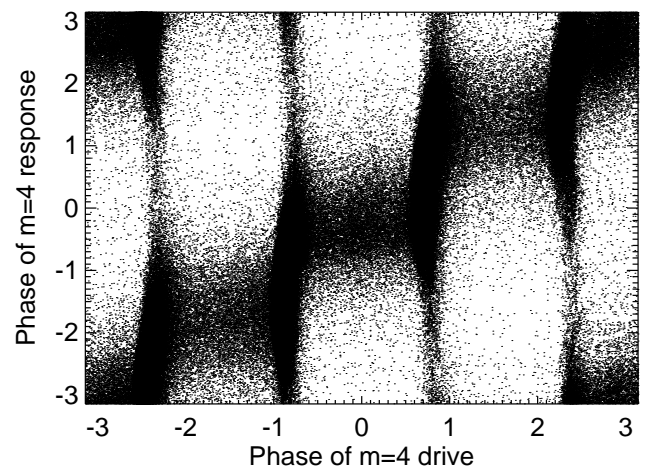


FIG. 16: Phase of the $m = 4$ drive vs. $m = 4$ response.

mode (i.e. in a resonant condition), with a peak value around $\pi/10$, confirming the existence of a partial phase synchronization, and becomes more and more flat as the frequency is moved away from the resonance condition. This can be observed in Fig. 17, where the phase difference distribution is plotted for different driving frequency values.

Finally, Fig. 18 shows the relative mode energy (i.e. the mode energy normalized to the total energy of the modes) for the case of an applied $m = 4$ mode in a resonant condition, along with that of the $m = 0, 3, 5$ modes, plotted as a function of the drive-response phase difference between the spontaneous and the induced fluctuations. It is possible to observe that when phase synchronization takes place, i.e. when the phase difference has a value around $\pi/10$, the relative amplitude of the driven mode ($m = 4$) is enhanced, while that of the other modes is reduced. Such a result is reminiscent of what found in Ref. [18], although it is not as strong (probably due to

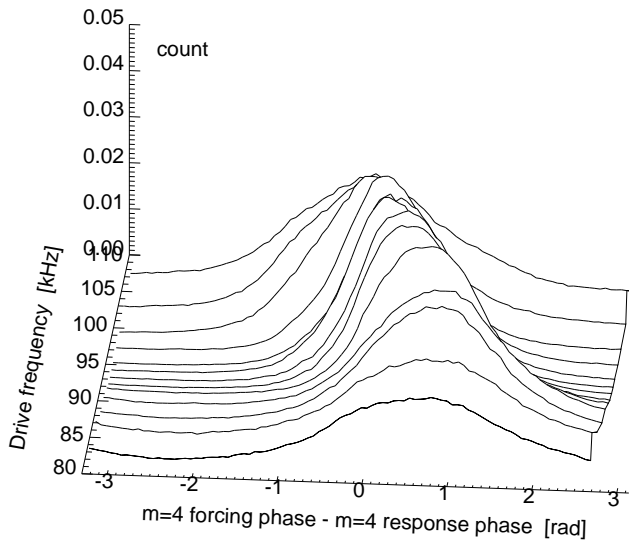


FIG. 17: Distribution of phase difference between the $m = 4$ drive and the $m = 4$ response for different values of the driving frequency.

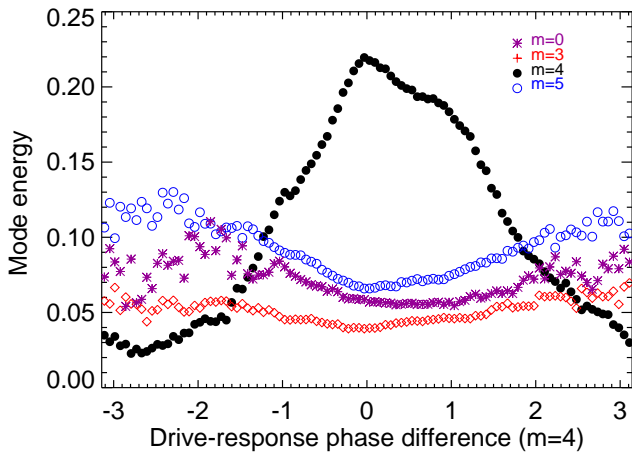


FIG. 18: Modes amplitude as a function of the phase difference between the $m = 4$ drive and the $m = 4$ response in resonant condition.

the drive weakness).

In order to further establish the existence of a partial phase synchronization, and its effect on the mode amplitude, we show in Fig. 19 a color-coded plot of the quantity

$$x(\theta, t) = A_m(t) \cos[m\theta + \alpha_m(t) - \alpha_{drive}(t)] \quad (2)$$

for $m = 4$, where $A_m(t)$ is the mode amplitude. This quantity is the $m = 4$ mode as seen in a reference frame moving with the applied voltage pattern [19]. The plot shows that a phase locking between drive and response is seen only in some time intervals, where a stationary pattern appears, and is lost in others, where the mode is found to move with respect to the applied perturbation.

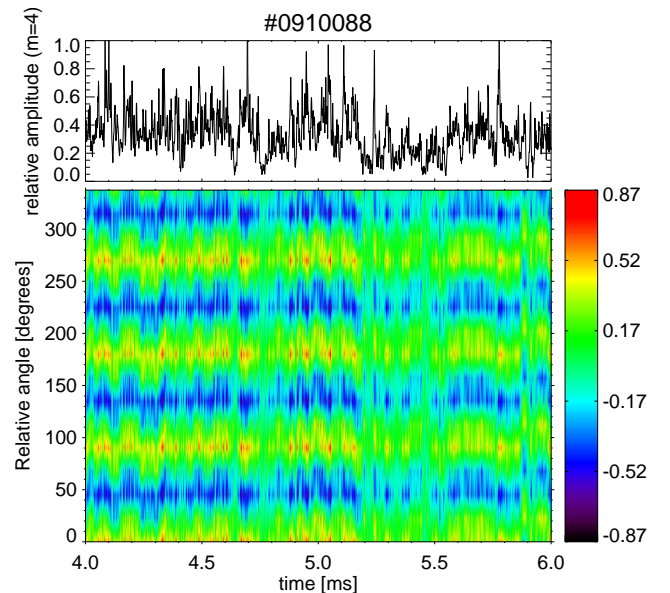


FIG. 19: $m = 4$ mode in the reference frame of the applied perturbation (bottom), and relative amplitude of it (top).

The top frame, showing the relative amplitude of the $m = 4$ mode, confirms that it increases during the phase synchronization intervals.

IV. CONCLUSION

The results of an experimental campaign aimed at controlling unstable electrostatic drift-waves in a low temperature magnetized plasma have been presented. Several mode numbers are observed on the spectrum of the floating potential fluctuation, which are not simultaneously present all the time, but tend to act as coupled oscillators, transferring energy from one to the other in an apparently chaotic fashion. By means of a local system of electrodes operating in electron current regime a wavelike pattern propagating has been induced in resonant condition (same phase velocity and frequency) with the naturally present modes. It has been observed that it is possible to increase the energy of one preferred mode, reducing the others, only if a good synchronization is obtained between the applied perturbation and the natural one. No effects on the broadband part of the spectrum can be seen, probably because the current collected by the electrodes is too small if compared to the total plasma current.

We plan to apply in the next future chaos control methods based on temporal (or spatiotemporal) feedback concepts, thus acting in closed-loop fashion in both space and time, to obtain, from an energetic point of view, less expensive effects on the plasma. This approach is intended as a test bed application of chaos and turbulence control techniques at the edge of thermonuclear fusion

Cathode radius	5 cm
Magnetic field (B)	14.2 mT
Operating pressure (P)	1 Pa
Plasma current (I)	0.6 A
Electron temperature (T_e)	2 eV
Ion temperature (T_i)	0.025 eV
Electron/ion density (n)	$2 \times 10^{17} \text{ m}^{-3}$
Ion cyclotron frequency (f_{ci})	5.4 kHz
Ion collision frequency (ν_i)	59 MHz
Electron cyclotron frequency (f_{ce})	400 MHz
Electron collision frequency (ν_e)	190 MHz

TABLE I: Main plasma parameters in the magnetron sputtering device.

devices, where electrostatic fluctuations are known to be responsible for anomalous particles transport, in order to improve confinement properties.

V. APPENDIX A

In this appendix, the deduction of the linear dispersion relation 1 will be briefly reminded. The first important point to consider is the low degree of ionization, of the order of 10^{-4} , of the plasma under study, where the collisions with neutral atoms dominate. The main parameters of the plasma under study are listed in Table I, where the collision frequencies have been evaluated by means of the expressions for their derivation reported in Ref. [20].

An important feature of this plasma is that only the electrons can be considered as magnetized. Indeed, given the measured plasma parameters, the electron and ion Larmor radius result $r_{Le} \sim 0.5$ mm and $r_{Li} \sim 10$ mm, respectively (the ion temperature in this non-thermal plasma can be assumed equal to that of the neutral gas, i.e. about 0.025 eV). These values must be compared to the mean free paths for electrons and ions λ_e , λ_i which are 20 and 90 mm, respectively [20]. As a consequence, the Hall parameter results $\gg 1$ for electrons and around 1 for ions in the magnetic trap volume. Therefore, ions are unmagnetized due to a Larmor radius comparable with their mean free path, whereas electrons are magnetized and are subjected to an $E \times B$ drift. The drifting electrons give rise to an azimuthal Hall current $I_{E \times B}$, roughly estimated as: $I_{E \times B} = en_e \pi a^2 E/B \sim 0.2A$, with a the radius of the equivalent circular cross-section for the azimuthal current. The corresponding magnetic field

evaluated at $r = a$ is: $B = \mu_0 I_{E \times B}/(2\pi a) \sim 4\mu T$, that is negligible compared with the values measured in the magnetic trap (Fig. 1).

In two previous papers [12, 13] we interpreted the observed electrostatic fluctuations in terms of an $\mathbf{E} \times \mathbf{B}$ /density gradient instability, also known as *neutral drag* instability. A linear dispersion relation was obtained for a low β_e , weakly ionized plasma, in a slab geometry with a straight magnetic field B along the z axis, the x axis being in the direction of the density and potential gradients. In such geometry the y direction corresponds to the azimuthal direction. The continuity equation for ions and electrons is considered:

$$\frac{\partial n}{\partial t} + \nabla \cdot (n\mathbf{v}_{e,i}) = Zn \quad (3)$$

along with their equations of motion, where electron inertia and the ion temperature T_i are neglected:

$$\frac{\partial \mathbf{v}_i}{\partial t} + (\mathbf{v} \cdot \nabla)\mathbf{v} = \frac{e}{M}(\mathbf{E} + \mathbf{v} \times \mathbf{B}) - \nu_i \mathbf{v} \quad (4)$$

$$0 = -\frac{T}{nm}\nabla n - \frac{e}{m}(\mathbf{E} + \mathbf{v} \times \mathbf{B}) - \nu_e \mathbf{v} \quad (5)$$

The right-hand side term of eq. 3 describe ionization events, with Z indicating the ionization rate. The same symbol n is used for electron and for ion densities (i.e. $n_e = n_i = n$), because quasineutrality is assumed due to the low frequency of the waves under consideration ($\omega/\omega_p \ll 1$, where ω_p is the electron plasma frequency). The neutral gas dynamics is assumed not to be affected by collisions of electrons and ions with neutrals.

By a standard procedure, which includes linearization, the dispersion relation:

$$\omega^2 + \omega \left[\frac{\Omega_i}{\nu_i} (k_x - \frac{\Omega_i}{\nu_i} k_y) v_E + i(\nu_i - Z) \right] - k^2 C_s^2 + Z\nu_i - i\Omega_i \left[\left(\frac{\Omega_i}{\nu_i} k_y - k_x \right) v_E + k_x v_{de} \right] = 0 \quad (6)$$

is thus determined (here C_s is the ion sound speed, $C_s \simeq (T_e/m)^{1/2}$, v_E is the $\mathbf{E} \times \mathbf{B}$ velocity, ν_i is the collision frequency of ions with neutrals, Ω_i is the ion cyclotron frequency multiplied by 2π , k is the wavevector and v_{de} is the electron diamagnetic drift speed $v_{de} = -T_e/(enB)(dn/dx)$).

[1] R. Nebel, J. Finn, *Proceedings of the 53rd Annual Meeting of the APS Division of Plasma Physics*, BP9.075, November 14-18, 2011, Salt Lake City, Utah.

[2] C. Schroder, T. Klinger, D. Block, A. Piel, G. Bonhomme and V. Naulin, *Phys. Rev. Lett.* **86**, 5711 (2001)

[3] C. Brandt, O. Grulke and T. Klinger, *Phys. Plasmas* **17**,

- 032304 (2010)
- [4] W. D. Suranga Ruhunusiri and J. Goree, *Phys. Rev. E* **85**, 046401 (2012)
- [5] D. W. Auerbach, T. A. Carter, S. Vincena, and P. Popovich, *Phys. Rev. Lett.* **105**, 135005 (2010)
- [6] J. A. Thornton, *J. Vac. Sci. Technol.* **15**, 171 (1978)
- [7] T. E. Sheridan and J. Goree, *J. Vac. Sci. Technol.* **A7**, 1014 (1989)
- [8] P. Kudrna, M. Holík, O. Bilyk, A. Marek, J. F. Behnke, E. Martines, and M. Tichý, *Proceedings of the XXVI International Conference on Phenomena in Ionized Gases*, Greifswald, 15-20 July 2003, edited by J. Meichsner, D. Loffhagen, H. E. Wagner Local Organizing Committee, Greifswald, 2003, Vol. 4, p. 157
- [9] A. P. Ehasarian *et al.*, *Appl. Phys. Lett.* **100**, 114101 (2012)
- [10] L. I and M. S. Wu, *J. Appl. Phys.* **62**, 4077 (1987)
- [11] C. Hidalgo, *Plasma Phys. Controlled Fusion* **37**, A53 (1995)
- [12] E. Martines, R. Cavazzana, G. Serianni, M. Spolaore, L. Tramontin, M. Zuin and V. Antoni, *Phys. Plasmas* **8**, 3042 (2001)
- [13] E. Martines, M. Zuin, V. Antoni, R. Cavazzana, G. Serianni, M. Spolaore and C. Nakashima, *Phys. Plasmas* **11**, 1938 (2004)
- [14] G. Serianni, L. Tramontin, M. Spolaore, V. Antoni, M. Bagatin, R. Cavazzana, D. Desideri and E. Martines, *XXIV International Conference on Phenomena in Ionized Gases* vol. 2, pag. 9, Warsaw, 11 - 16 July 1999, ed. P. Pisarczyk, T. Pisarczyk, J. Wolowski (Polish Academy of Sciences, Warsaw, 1999)
- [15] J. W. Bradley, S. Thompson, and Y. A. Gonzalvo, *Plasma Sources Sci. Technol.* **10**, 490 (2001)
- [16] C. Chandre, G. Ciraolo, F. Doveil, R. Lima, A. Macor, and M. Vittot, *Phys. Rev. Lett.* **94**, 074101 (2005)
- [17] F. Doveil, Kh. Auhmani, A. Macor, and D. Guyomarch, *Phys. Plasmas* **12**, 010702(L) (2005)
- [18] T. Klinger, A. Latten, A. Piel, G. Bonhomme, T. Pierre, T. and T. Dudok de Wit, *Phys. Rev. Lett.* **79**, 3913 (1997)
- [19] D. Block, A. Piel, Ch. Schröder, and T. Klinger, *Phys. Rev. E* **63**, 056401 (2001)
- [20] M. A. Lieberman and A. J. Lichtenberg, *Principles of Plasma Discharges and Material Processing* (Wiley and Sons, New York, 1994)